Direct evidence of magnetostructural phase separation in the electron-doped manganite $Ca_{0.8}Sm_{0.16}Nd_{0.04}MnO_3$ by means of high magnetic field studies

F. Duc,[1] J. Vanacken,[2] G. Zhang,[2] W. Decelle,[2] J. E. Lorenzo,[3] C. Detlefs,[4] C. Strohm,[3,4] T. Roth,[4] R. Suryanarayanan,[5] P. Frings,[1] and G. L. J. A. Rikken[1]

[1]*Laboratoire National des Champs Magnétiques Intenses, CNRS-INSA-UJF-UPS, 143 Avenue de Rangueil, F-31400 Toulouse, France*

[2]*Pulsveldengroep, Institute for Nanoscale Physics and Chemistry, Celestijnenlaan 200D, B-3001 Leuven, Belgium*

[3]*Institut Néel, CNRS, Boîte Postale 166X, F-38043 Grenoble Cedex, France*

[4]*European Synchrotron Radiation Facility, Boîte Postale 220, F-38043 Grenoble Cedex, France*

[5]*Laboratoire de Physico-Chimie de l'Etat Solide, Bât 410, Université Paris-sud, F-91405 Orsay, France*

(Received 19 May 2010; revised manuscript received 9 July 2010; published 10 August 2010)

The structural and magnetic properties of $Ca_{0.8}Sm_{0.16}Nd_{0.04}MnO_3$ have been investigated by synchrotron x-ray powder diffraction in pulsed magnetic fields in connection with resistivity and magnetization measurements (in static and pulsed magnetic fields). Below 100 K, the spontaneous ($B=0$) low-temperature phase is found to be structurally and magnetically phase segregated, a major antiferromagnetic monoclinic $P2_1/m$ phase coexisting with a minor antiferromagnetic orthorhombic *Pnma* phase containing ferromagnetic clusters. Upon the application of a magnetic field, two magnetic transitions occur: a first transition without structural changes at low field, showing the superparamagnetic like behavior of ferromagnetic domains, followed by a metamagnetic transition. The latter is clearly accompanied by field-induced structural changes, the orthorhombic phase growing at the expense of the monoclinic one.

DOI: 10.1103/PhysRevB.82.054105 PACS number(s): 75.25.−j, 75.47.Gk, 75.60.−d

I. INTRODUCTION

The physical properties of manganite compounds, $R_{1-x}D_xMnO_3$ (R=rare-earth La, Nd, Sm; D=alkaline-earth metals Sr, Ca, Ba,…), such as colossal magnetoresistance (CMR) effect, charge ordering, orbital ordering and phase separation have been extensively studied during the last ten years. These properties can be tuned by changing the nature and the concentrations of the trivalent rare-earth and divalent alkaline-earth cations, which determine both the distortion of the crystalline perovskite structure ABO_3 and the concentration of e_g electrons at the Mn sites.

The interplay between charge, spin, lattice and orbital degrees of freedom in these compounds is the source of very rich phase diagrams in which several structural and magnetic phases have been observed. One of the main results of the research in manganite type compounds is the discovery of a strong tendency toward *phase separation*, i.e., the formation of inhomogeneous states. This result is very robust, appearing both in experiments and in theoretical models.[1] The colossal magnetoresistance effect appears to be closely linked to these mixed phase tendencies and to the strong competition between the ferromagnetic (FM) metallic state and the antiferromagnetic (AF) insulating state which supports charge and orbital order.

An interesting type of phase separation occurs in the electron-doped manganite $Ca_{0.85}Sm_{0.15}MnO_3$. At room temperature it is a paramagnetic semimetal with orthorhombic space group *Pnma*. Below 130 K, it exhibits magnetostructural phase separation. Two long-range AF phases coexist down to 5 K: a minor orthorhombic (*Pnma*) phase with *G*-type magnetic order, and a major monoclinic ($P2_1/m$) phase with *C*-type magnetic order.[2] Interestingly, the CMR effect is observed only for compositions in the vicinity of the boundary between the cluster-glass-type state ($x>0.85$) and charged-ordered AF state ($x<0.85$).[3] For temperatures lower than 112 K, this compound undergoes a metamagnetic transition, associated with a field-induced structural transition.[4–8] This structural transformation was first revealed by neutron diffraction experiments in steady magnetic field up to 6 T,[6] and further corroborated by magnetization and resistivity measurements.[7,8] These field-induced magnetic and crystallographic transitions have been attributed to the coexistence of different metastable states with very similar energies.[6,8]

In the present work, we have investigated the structural and magnetic behavior of an electron-doped manganite of the $Ca_xSm_{1-x}MnO_3$ series at magnetic fields up to 30 T. To that end we have performed synchrotron x-ray powder diffraction under pulsed magnetic fields,[9] combined with resistivity and magnetization measurements. We have carried out these experiments on a sample of $Ca_{0.8}Sm_{0.16}Nd_{0.04}MnO_3$. An additional substitution by Nd has been inserted at the *A*-site of the perovskite structure in order to study the role of extra disorder (discussed in detail in Ref. 10) on the magnetostructural phase separation.

II. EXPERIMENTAL METHODS

A. X-ray experiments

X-ray powder diffraction experiments in high pulsed magnetic field were performed with synchrotron radiation on the magnetic scattering beamline, ID20, at the ESRF.[11] Experimental conditions and configuration were those previously described in detail in Ref. 9 with some improvements described below. Photons emitted from an undulator source were monochromatized by a Si(111) double crystal monochromator tuned to 21 keV ($\lambda=0.59$ Å). Pulsed magnetic fields up to 30 T were provided by a magnet and cryostat assembly that was custom-built for these experiments at the

LNCMI-Toulouse, France. The magnet coil, optimized for powder diffraction, exhibits conical ends with an opening angle of 40°.[12] It was horizontally mounted into a cryostat so that the beam axis was along the bore of the magnet (Faraday geometry).

The magnetic field pulse length was ~20 ms. The diffraction patterns presented in this work were exclusively recorded at the maximum of the magnetic field pulse, spanning 3.4 ms. The x-rays exposure time was defined by a fast mechanical shutter synchronized with the pulsed field. The magnet and the cryostat assembly were installed downstream of this shutter, followed by the detector, a Rigaku R-axis IV++ image plate.[13] The resolution of the plate used was 100 μm between two pixels, and the total detection area was 300×300 mm^2. The sample-detector distance was set to 0.45 m to resolve the splitting induced by the spontaneous symmetry changes.

A polycrystalline sample of $Ca_{0.8}Sm_{0.16}Nd_{0.04}MnO_3$ was synthesized as described elsewhere.[10] It was embedded into a resin (polyvinylpyrrolidone) in order to prevent grain movement. These displacements, albeit tiny, may affect the reproducibility of the powder diffraction data and thus complicate data analysis. The sample thickness was adjusted to about one absorption length at the working energy.

Diffraction patterns were extracted from the raw images by using the software packages FIT2D (Refs. 14 and 15) and analyzed by means of the refinement program FULLPROF (Ref. 16) using the Rietveld method.

B. Magnetization experiments

Sample magnetization measurements have been carried out in pulsed magnetic fields up to 40 T, and in constant magnetic fields up to 12 T. During a pulsed field magnetization measurement (PFMM), a 25 ms magnetic field pulse of up to 40 T was applied while the susceptibility of the sample is simultaneously measured by means of a calibrated susceptometer (compensated coils method). The sample can be removed *in situ* to perform sample in/out measurement sequences for compensating parasitic inductive voltages. The sensitivity of this in-house designed susceptometer is better than 10^{-3} emu at fields below 20 T and 10^{-2} emu at higher fields. The measurements in a direct current (dc) magnetic field were performed with a standard Oxford Instruments vibrating sample magnetometer (VSM), using a vibration frequency of 55 Hz and a Foner detection coil assembly. The transport measurements were performed using a four point contact technique, and switching the current polarity to avoid parasitic thermocouple voltages.

III. RESULTS AND DISCUSSION

A. Pulsed magnetic field x-ray powder diffraction

First, the temperature dependence of x-ray powder diffraction patterns has been recorded at zero field, as shown in Fig. 1. Their detailed analysis shows that part of the sample undergoes a structural phase change from orthorhombic (*Pnma*) at room temperature to monoclinic ($P2_1/m$) below 130 K, in agreement with previous results on

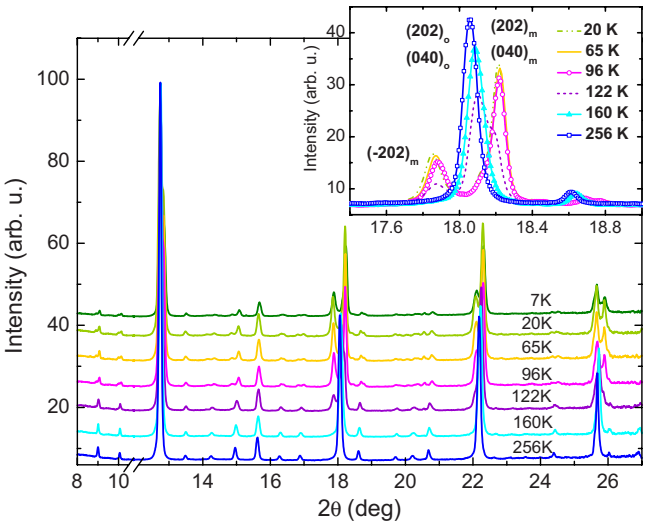

FIG. 1. (Color online) Temperature dependence (from 7 to 256 K) of synchrotron x-ray powder diffraction patterns observed for $Ca_{0.8}Sm_{0.16}Nd_{0.04}MnO_3$. The inset shows the (202)/(040) reflections that are sensitive to the monoclinic distortion. The orthorhombic and monoclinic reflections are indicated by the subscripts "*o*" and "*m*," respectively.

$Ca_{0.85}Sm_{0.15}MnO_3$.[2] Between 130 and 100 K, the volume fraction of the $P2_1/m$ phase increases gradually at the expense of the orthorhombic one, reaching 34(1)% at 122 K and achieving finally 85(1)% at 96 K. Below 100 K, the fraction of each phase remains unchanged indicating that the structural transition is completed. The amount of the remaining orthorhombic phase in $Ca_{0.8}Sm_{0.16}Nd_{0.04}MnO_3$ is however higher than in $Ca_{0.85}Sm_{0.15}MnO_3$, reaching 15% instead of 6% as suggested by previous experiments.[2] We attribute this enhancement of the structural phase separation to the additional substitution by Nd.

The evolution of cell parameters and volume as a function of temperature are shown in Fig. 2. Below 100 K, only the monoclinic cell parameters have been reported even if both phases are still present.

Next, we have investigated the evolution of the diffraction patterns as a function of the applied magnetic field. A series of magnetic field x-ray measurements (from 0 to 30 T in 5 T steps) were carried out from low temperature to high temperature. To detect potential systematic errors, field spectra were recorded before and after each series of magnetic field pulses. No displacements of the whole pattern, or variation in the intensity of various peaks were detected, indicating the absence of significant grain movements.

The field dependence of the diffraction spectra measured at $T=7$ K is reported in Fig. 3. At this temperature, $Ca_{0.8}Sm_{0.16}Nd_{0.04}MnO_3$ is mainly monoclinic. The field-induced structural transition is clearly visible: under the applied magnetic field, the monoclinic $P2_1/m$ structure is gradually transformed into the orthorhombic *Pnma* phase. This transformation is however not complete even at 28.7 T. Low intensity peaks of the monoclinic phase are still present in the recorded patterns, as illustrated by the monoclinic (−202), (202), and (040) reflections observed in Fig. 3.

Detailed analysis of diffraction profiles allows the determination of the fraction of each phase as a function of the

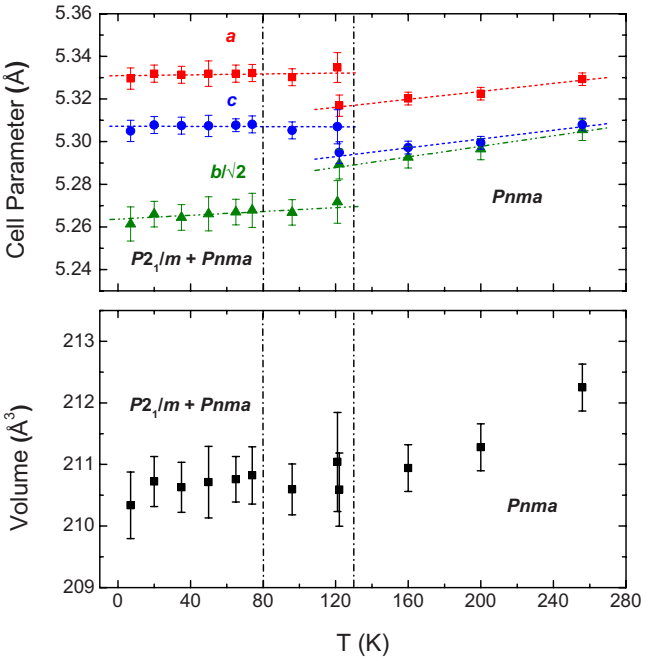

FIG. 2. (Color online) Temperature dependence of lattice parameters (top) and unit cell volume (bottom) of $Ca_{0.8}Sm_{0.16}Nd_{0.04}MnO_3$. Below 100 K, only the monoclinic parameters are reported. The monoclinic angle β is equal to 91°.

applied magnetic field. The results are displayed in Fig. 4. The orthorhombic phase fraction increases with magnetic field at the expense of the monoclinic one, reaching around 85% at 28.7 T. Below 100 K, the fraction of each phase is determined by the value of the magnetic field and shows only small variations with temperature. This indicates that the field-induced structural transition in this electron-doped manganite is directly related to its magnetic properties. At 122 K, which is in the temperature range where the spontaneous structural transition occurs, 2/3 of the sample is already orthorhombic at zero field. A magnetic field of 19.1 T is sufficient to induce a nearly complete transformation into

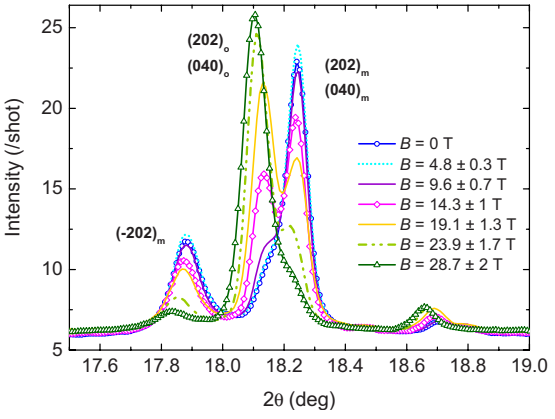

FIG. 3. (Color online) Field dependence (0 to 30 T from top to bottom) of synchrotron x-ray powder diffraction pattern observed for $Ca_{0.8}Sm_{0.16}Nd_{0.04}MnO_3$ at $T=7$ K. The value of the magnetic field for each shot and its standard deviation were determined by averaging the values taken during the 3.4 ms exposure window.

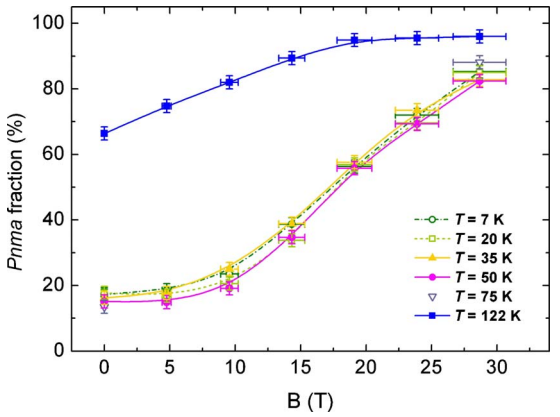

FIG. 4. (Color online) Orthorhombic phase fraction vs B and T. The lines are only a guide to the eye.

the orthorhombic *Pnma* phase, although 5% of the AF monoclinic phase still remains and coexists with the orthorhombic one. The field dependence of the diffraction patterns at high temperatures (160 K $\leq T \leq$ 256 K) have been also investigated. No symmetry change was detected and the system displays the orthorhombic *Pnma* structure. No significant variations were observed on the lattice parameters and unit cell volume as a function of field.

B. Magnetic field magnetization and resistive measurements

The temperature dependence of the resistivity and the magnetization are shown in Fig. 5. A clear, although broad, transition at around $T_{mid}=113$ K is observed, with the onset at $T=130$ K and saturation at $T=80$ K. This is the same temperature range where diffraction experiments have signaled an orthorhombic to monoclinic phase transition. Note that the resistivity data were taken at zero field whereas a small field of $B=0.01$ T was applied to obtain the magneti-

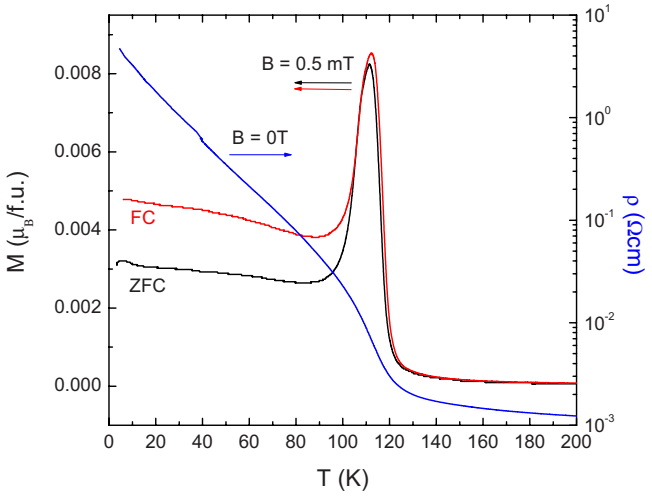

FIG. 5. (Color online) Temperature dependence of the resistivity ($B=0$ T) and ZFC and FC magnetization at $B=0.5$ mT of $Ca_{0.8}Sm_{0.16}Nd_{0.04}MnO_3$. The structural transition (80–130 K) which is shown in Fig. 2 is clearly observed via the resistivity and the magnetization.

zation curve. On lowering the temperature a gradual increase in the resistivity can be observed in the log-lin $\rho-T$ plot. Although the magnetization decreases again after the transition, the resistivity continues to increase. Two distinct regimes can be identified, one above the transition (300 K $\rightarrow$130 K) and one below the transition (80 K$\rightarrow$20 K). In the vicinity of the transition the resistivity goes gradually from one regime to the other. Below $T=20$ K the resistivity can best be fitted by the logarithmic divergence $\rho \propto \log(1/T)$ characteristic of an additional Kondo-like scattering.

The magnetization above the transition, and during the main part of the transition, is reversible, since both the zero field cooling (ZFC) and field cooling (FC) curves virtually coincide. Below the transition (about $T<$ 100 K) an irreversibility clearly occurs that is either a consequence of (i) a phase separation/reorganization of phase domains or (ii) a result of the FM phase which is irreversible on its own.

The resistivity curve presented in Fig. 5 increases from high to low temperature. This effect is due to the presence of AF regions, which are $P2_1/m$ phase, arising out of the paramagnetic *Pnma* phase. The AF areas are mostly insulating where charge transport is hindered by the ever changing spins of the manganite. The magnetization at high temperature follows a simple paramagnetic law as shown by the typical straight line from 300 K down to the transition area ($\approx$175 K) in the $1/\chi$ plot (not reported). In the high temperature regime (below $\approx$175 K), a small irreversibility occurs since both FC and ZFC curves do not exactly coincide. The occurrence of a small irreversibility at high temperatures is best revealed in the small hysteresis in the ρ vs B data shown in Fig. 6. We believe that the presence of small (possibly mobile) FM droplets mixed in the paramagnetic background can account for this behavior. Below 100 K the difference between ZFC and FC modes is more apparent. On lowering the temperature in the presence of the magnetic field ($B=0.5$ mT), the moments are distinctly larger than when zero field cooled (care was taken in sweeping out the remnant field of the superconducting magnet used to apply the external field in the VSM).

Figure 6 shows the magnetoresistance at different temperatures, above and below the transition. At $T=150$ K the resistivity is small, and so is the irreversibility in the $\rho-B$ curve. This is consistent with a predominantly paramagnetic phase at this temperature.

We can assume that the average magnetization vector in the paramagnetic phase scales with the Brillouin function $\mathcal{B}_J(x)$ [with $x=g\mu_B J(T)B/k_BT$]. $J(T)$ in this case is the average spin moment of the magnetic clusters at the hopping sites, $g=2$ is the Landé g factor of Mn and μ_B is the Bohr magneton. Let W be the difference between the energy barriers for hopping of charge carriers between clusters with random mutual spin orientation, and for hopping between spin-aligned clusters. When the applied field $B=0$, the spins of the clusters are randomly distributed and the hopping barrier has a maximum value [$W\mathcal{B}_J^2(x)=0$]. When an external field is applied (B is non zero) and the hopping barrier reduces by $W\mathcal{B}_J^2(x)>0$. Finally, when all clusters have aligned spins, $\mathcal{B}_J^2=1$ and the total hopping barrier is reduced by W. This leads to the following equation for the spin dependent hopping,[17]

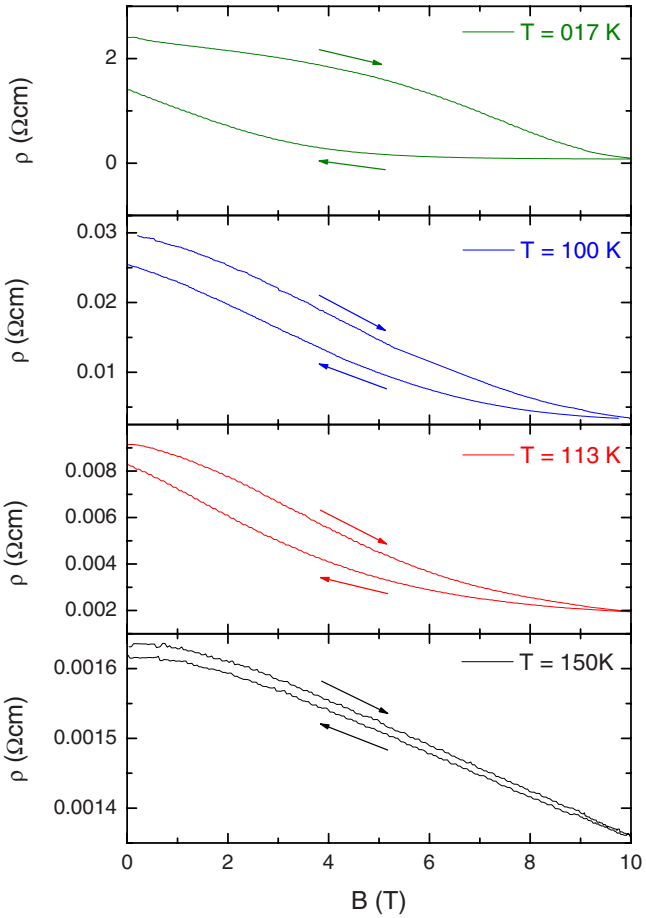

FIG. 6. (Color online) Magnetoresistivity indicating irreversible behavior, which increases as the temperature lowers from $T=150$ K$\rightarrow T=113$ K$\rightarrow T=100$ K$\rightarrow T=17$ K.

$$\rho(B) = \rho(0)\exp\left(\frac{-W\mathcal{B}_J^2(x)}{k_BT}\right). \quad (1)$$

Taking this function, the PM high temperature data set can be fitted using the following fitting parameters: $J=26.7$ and $W=0.974\times10^{-21}$ J($\approx$70 K).

Although the model is also capable to fit data in the FM state, we must notice that, in our case, the fraction of FM regions is constantly changing as a function of the applied magnetic field, due to the phase separation. This can easily be seen from the x ray and from the magnetization data. For this reason, all attempts to fit these (strongly hysteretic) data fail. The magnetoresistivity is then better described by using a percolation-type transport. A FM like percolating part grows as the field is increased, and allows good electrical transport through the AF insulating background. Furthermore, this FM fraction is remnant after the field is turned off again, leading to a distinct hysteresis in our presented data (Fig. 6).

Figure 7 shows the magnetization versus field, measured in a pulse of 25 ms. Three different temperatures are shown, one above, one intermediate and one below the transition temperature. At high temperature, a Brillouin-like magnetization curve, typical for a paramagnetic phase, is observed. On lowering the temperature, two distinct transitions occur.

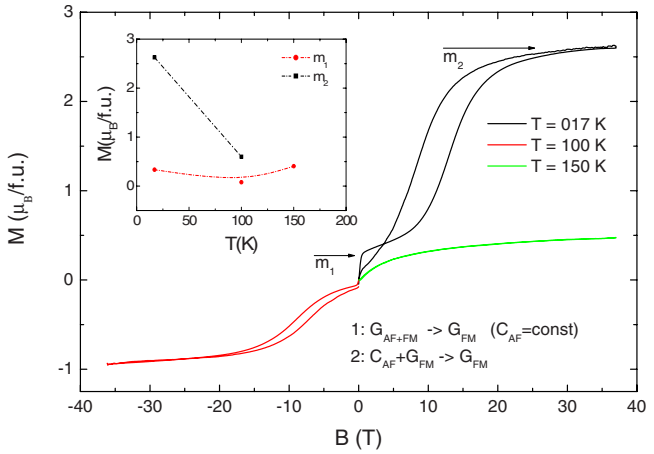

FIG. 7. (Color online) M vs B hysteresis measurements at different temperatures (T=150 K, T=100 K, and T=17 K). At low temperatures, two distinct phases can be observed. The temperature dependence of their fractions are shown in the inset.

First a step (m_1) at relative low magnetic field, followed by a broad transition (m_2) at higher fields (5 T→25 T). The interpretation of these results is again quite straightforward. At the fast transition, the superparamagnetic like or FM droplets, magnetically insulated by the paramagnetic phase, easily switch to be aligned parallel to the field direction. These particles are still in the *Pnma* structural phase. When the field is further increased the FM phase becomes dominant with a concomitant disappearance of the AF phase.

The magnetization data presented in Fig. 8 shows that up to the first transition (m_1), the hysteresis is small. Only at higher fields, which cause the AF phase to be converted into the FM phase, the large irreversibility becomes evident. This

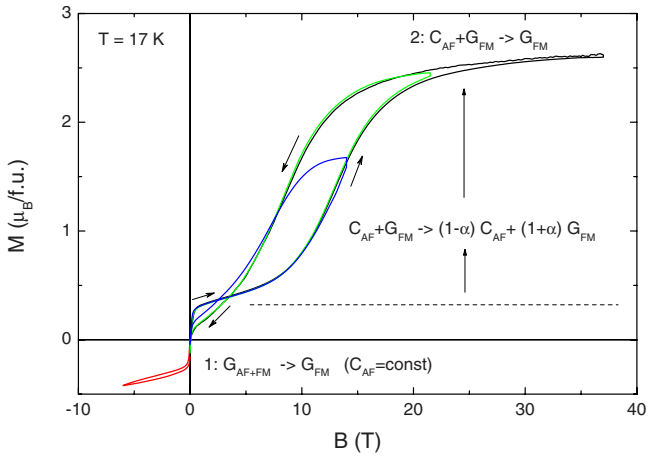

FIG. 8. (Color online) M vs B hysteresis measurements at T =17 K. Magnetic fields of different magnitudes were applied, reaching values of (−)6, 14, 22, and 37 T. Positive/negative field polarities are shown for clarity only.

latter step could cause sample heating and thus explain why the magnetization of the lowering field branch is lower than that of the rising field branch.

IV. CONCLUSIONS

In summary, we have investigated the temperature and magnetic field effects on the structural and magnetic properties of the electron-doped manganite $Ca_{0.8}Sm_{0.16}Nd_{0.04}MnO_3$. Upon lowering the temperature through 113 K, this compound exhibits a first order structural and magnetic transition, associated with a metal-insulator transition.

Below 130 K, both low field magnetization data and zero field synchrotron powder diffraction evidence the coexistence and competition of two magnetic and structural phases: a major monoclinic state with AF magnetic order and a minor orthorhombic phase containing FM clusters, as previously observed in $Ca_{0.85}Sm_{0.15}MnO_3$. In the high temperature regime, our magnetoresistivity data indicate the presence of small FM droplets included in the paramagnetic phase. On lowering the temperature through the transition, the compound goes from a paramagnetic phase with small FM inclusions to a mainly AF phase with small FM domains. To behave as individual non coupled FM particles, the FM droplets should be separated from the AF phase by a paramagnetic buffer layer. The latter would avoid exchange bias like effect that should make the reorientation of the FM droplets inside the AF matrix difficult. On applying a small magnetic field, the superparamagnetic like droplets then easily switch to be aligned to the field direction (transition m_1). When the field is further increased, the FM domains become dominant gradually at the expense of the AF ones (transition m_2). This magnetic transition is concomitant with the increase of the orthorhombic phase fraction with the magnetic field, demonstrating that the field-induced structural transformation is strongly related to the metamagnetic transition. Our experiments are consistent with earlier observations,[6–8] which in the high field region lacked the sensitivity to the structural component of the metamagnetic transition.

In conclusion, our experiments have given macroscopic and microscopic evidence of magnetic and structural phase separation in the electron-doped manganite $Ca_{0.8}Sm_{0.16}Nd_{0.04}MnO_3$. The phase separation persists for all field values investigated, crossing a maximum with 50% of both phases at 17–18 T.

ACKNOWLEDGMENTS

The authors thank A. Fondacaro and C. Mazzoli from ID20 beamline for help in setting up this experiment. The assistance of M. Nardone to repair the He flow cryostat during the beamtime was greatly appreciated. The safety issues of the equipment were addressed with the help of ESRF safety group. We acknowledge the European Synchrotron Radiation Facility for provision of beamtime through the peer-reviewed long term Project No. HS2788. Part of this research was funded by the ANR (Grant No. ANR-05-BLAN-0238).

[1] E. Dagotto, T. Hotta, and A. Moreo, Phys. Rep., Phys. Lett. **344**, 1 (2001).
[2] C. Martin, A. Maignan, M. Hervieu, B. Raveau, Z. Jirak, A. Kurbakov, V. Trounov, G. Andre, and F. Bouree, J. Magn. Magn. Mater. **205**, 184 (1999).
[3] M. Respaud, J. M. Broto, H. Rakoto, J. Vanacken, P. Wagner, C. Martin, A. Maignan, and B. Raveau, Phys. Rev. B **63**, 144426 (2001).
[4] C. Martin, A. Maignan, F. Damay, M. Hervieu, and B. Raveau, J. Solid State Chem. **134**, 198 (1997).
[5] R. Mahendiran, A. Maignan, C. Martin, M. Hervieu, and B. Raveau, Phys. Rev. B **62**, 11644 (2000).
[6] P. A. Algarabel, J. M. De Teresa, B. Garcia-Landa, L. Morellon, M. R. Ibarra, C. Ritter, R. Mahendiran, A. Maignan, M. Hervieu, C. Martin, B. Raveau, A. Kurbakov, and V. Trounov, Phys. Rev. B **65**, 104437 (2002).
[7] D. A. Filippov, R. Z. Levitin, A. N. Vasil'ev, T. N. Voloshok, H. Kageyama, and R. Suryanarayanan, Phys. Rev. B **65**, 100404(R) (2002).
[8] A. S. Lagutin, J. Vanacken, A. Semeno, Y. Bruynseraede, and R. Suryanarayanan, Solid State Commun. **125**, 7 (2003).
[9] P. Frings, J. Vanacken, C. Detlefs, F. Duc, J. E. Lorenzo, M. Nardone, J. Billette, A. Zitouni, W. Bras, and G. L. J. A. Rikken, Rev. Sci. Instrum. **77**, 063903 (2006).
[10] D. A. Filippov, K. V. Klimov, R. Z. Levitin, A. N. Vasil'ev, T. N. Voloshok, and R. Suryanarayanan, J. Phys.: Condens. Matter **15**, 8351 (2003).
[11] L. Paolasini, C. Detlefs, C. Mazzoli, S. Wilkins, P. P. Deen, A. Bombardi, N. Kernavanois, F. de Bergevin, F. Yakhou, J. P. Valade, I. Breslavetz, A. Fondacaro, G. Pepellin, and P. Bernard, J. Synchrotron Radiat. **14**, 301 (2007).
[12] J. Billette (unpublished).
[13] T. Fujisawa, Y. Nishikawa, H. Yamazaki, and Y. Inoko, J. Appl. Crystallogr. **36**, 535 (2003).
[14] A. P. Hammersley, S. O. Svensson, M. Hanfland, A. N. Fitch, and D. Hausermann, High Press. Res. **14**, 235 (1996).
[15] A. P. Hammersley, *Fit2D V9.129 Reference Manual V3.1, Internal Report ESRF98HA01T* (1998).
[16] J. Rodríguez-Carvajal, Physica B **192**, 55 (1993).
[17] P. Wagner, I. Gordon, L. Trappeniers, J. Vanacken, F. Herlach, V. V. Moshchalkov, and Y. Bruynseraede, Phys. Rev. Lett. **81**, 3980 (1998).